Subliminal Reorientation and Repositioning in Immersive Virtual Environments using Saccadic Suppression

Benjamin Bolte and Markus Lappe

Abstract—Virtual reality strives to provide a user with an experience of a simulated world that feels as natural as the real world. Yet, to induce this feeling, sometimes it becomes necessary for technical reasons to deviate from a one-to-one correspondence between the real and the virtual world, and to reorient or reposition the user's viewpoint. Ideally, users should not notice the change of the viewpoint to avoid breaks in perceptual continuity. Saccades, the fast eye movements that we make in order to switch gaze from one object to another, produce a visual discontinuity on the retina, but this is not perceived because the visual system suppresses perception during saccades. As a consequence, our perception fails to detect rotations of the visual scene during saccades. We investigated whether saccadic suppression of image displacement (SSID) can be used in an immersive virtual environment (VE) to unconsciously rotate and translate the observer's viewpoint. To do this, the scene changes have to be precisely time-locked to the saccade onset. We used electrooculography (EOG) for eye movement tracking and assessed the performance of two modified eye movement classification algorithms for the challenging task of online saccade detection that is fast enough for SSID. We investigated the sensitivity of participants to translations (forward/backward) and rotations (in the transverse plane) during trans-saccadic scene changes. We found that participants were unable to detect approximately ± 0.5m translations along the line of gaze and $\pm 5^\circ$ rotations in the transverse plane during saccades with an amplitude of 15°. If the user stands still, our approach exploiting SSID thus provides the means to unconsciously change the user's virtual position and/or orientation. For future research and applications, exploiting SSID has the potential to improve existing redirected walking and change blindness techniques for unlimited navigation through arbitrarily-sized VEs by real walking.

Index Terms—Reorientation, repositioning, saccadic suppression, detection thresholds, eye tracking, electrooculography.

1 Introduction

Immersive virtual environments (VEs) often consists of head-mounted displays (HMDs) as well as position and orientation tracking systems. These devices enable the transfer of real body movements into virtual worlds, which in turn allows the user to navigate through VEs by real walking. Walking is the most basic, intuitive and direct way of moving in the real world compared to interaction devices such as gamepads [34]. Therefore, navigation through VEs by real walking is highly desirable. Straightforward mapping of the body movements of users to the virtual camera, however, restricts the user's movements to the limited dimension of the tracked space in which the user moves.

These restrictions can be tackled by developing either hardware devices that prevent a displacement in the real world or software approaches that use a more elaborate mapping of user's movements to the virtual camera. Several prototypes of hardware devices have been developed to support unlimited walking in immersive VEs, such as torus-shaped omni-directional treadmills [3, 28], motion foot pads [16], motion carpets [27] and stroller-based walking platforms [32]. Cheaper devices that target the consumer sector, such as the Virtuix Omni, are currently becoming available. However, these devices have drawbacks. They occupy space even when not used. They require practice to maintain balance. They restrict movement due to mechanical parts that are necessary for safety purposes.

Software approaches to unlimited walking in arbitrarily-sized immersive VEs are a cost-effective and practical alternative to hardware devices. Repositioning [36, 37] and reorientation [22, 30] techniques support navigation by real walking in moderately large virtual worlds. Reorientation techniques, additionally, ensure the safety of users by rotating them away from obstacles such as the boundaries of the available tracking space. Therefore, reorientation techniques are typically also used in other software approaches, as a fall-back to avoid collisions in case the approach fails to restrict the user's movements inside the boundaries of the available space. For example, redirected walking techniques [5, 24] often rely on reorientation techniques as a fall-back, since typical tracking spaces are smaller than the required space for unnoticeable redirection [12, 24, 29]. Since users seem to prefer those reorientation approaches that avoid introducing breaks in presence such as virtual distractors [22], it is desirable that the reorientation is unnoticeable for users.

The perceptual phenomenon of saccadic suppression of image displacement (SSID) offers the opportunity to subliminally reposition and reorient users. During rapid saccadic eye movements, the visual system fails to detect small changes of the visual scene [4, 8]. Although the scene changes for individual saccades may only be small, total changes summed-up over several saccades may quickly become large since humans normally perform on average 3 saccades per second.

We combined an electrooculography (EOG) tracker with an HMD and assessed the performance of two modified eye movement classification algorithms for online saccade detection that is fast enough to change the scene during saccades. We then investigated how much participants can be translated (forward/backward) and rotated (in the transverse plane) without noticing trans-saccadic scene changes.

Our intention with the proposed approach of exploiting SSID for future research and applications is to improve existing redirected walking and change blindness techniques. For instance, saccadic suppression could be used to mask scene changes in the visual illusions approach [6] instead of distracting gray screens. Saccadic suppression may also be used to change the position of doors, without requiring the user to turn away, for change blindness techniques such as the one proposed by Suma et al. [31]. Trans-saccadic scene translations and rotations could be applied in addition to curvature gains, which might reduce the required space for unnoticeable redirected walking.

2 Related Work

2.1 Saccadic Suppression of Image Displacement

Saccades are brief and fast eye movements that we make in order to direct gaze from one object to another. Typically, one saccade is made

- *Benjamin Bolte is with University of Muenster. E-mail: b.bolte@uni-muenster.de.*
- *Markus Lappe is with University of Muenster. E-mail: mlappe@uni-muenster.de.*

Manuscript received 18 Sept. 2014; accepted 10 Jan. 2015. Date of Publication 20 Jan. 2015; date of current version 23 Mar. 2015. For information on obtaining reprints of this article, please send e-mail to: reprints@ieee.org.

every 300–400ms. Saccades can be made voluntarily, for example if one is asked to look at an object pointed out by someone else, or involuntarily, for example if something suddenly enters the field of view. They induce a burst of large field visual motion on the retina and a sudden change of the retinal scene from before to after the movement. Neither the induced visual motion nor the changes of the view of the scene are consciously perceived. Instead, our percept is that of a continuous, stable and uninterrupted surrounding space. Saccadic suppression of image displacement (SSID) is one of the mechanisms that the visual system uses to create this percept of visual stability. It means that perception of displacement of the scene during a saccade is suppressed, or, more precisely that thresholds for detection of a displacement of the current retinal image are elevated when this displacement occurs during a saccade [4]. According to current theories, the human visual system uses a built-in prior assumption that the world is stable during eye movements. Therefore, differences between the actual gaze direction after the saccade and the intended target direction are more likely due to an imprecise saccade than to a displacement of the world [19]. Usually, SSID is studied using isolated targets on a computer screen that are displaced in or against saccade direction. Threshold elevations are smaller for displacements orthogonal to saccade direction [19]. However, saccadic suppression is not restricted to displacements of the scene. Detection of changes of elements in the scene is also impaired during saccades [13].

Saccadic suppression is tightly linked to the time course of saccades. Threshold elevation begins about 50ms before saccade onset, peaks at saccade onset and is almost finished when the saccade ends [10]. In fact, when a brief delay period is introduced after the saccade, displacements become easily visible [9]. It is therefore important to temporally align the displacement with the saccade onset.

Triesch et al. [33] described and evaluated a system to exploit SSID by combining a limbus eye tracker for fast online saccade detection and a video-based eye tracker for high accuracy. The system proved to be usable in VR setups but vertical head movements easily corrupted the calibration of the limbus tracker. Schumacher et al. [26] described a system using solely a video-based eye tracker for exploiting SSID in CAVE setups to mask interactive graphic updates. Using the same system, Herpers et al. [14] found that participants perceived trans-saccadic horizontal translations of natural scene images as smaller compared to similar translations when no saccade was performed. Probability to detect scene changes of high-resolution real world images was determined for 3 (leftwards/rightwards) scene translation amplitudes. Due to the low temporal resolution of 120Hz of the video-based eye tracker, undetectable scene changes could be applied only for large saccades. The false alarm rate of 20% would be too high for subliminal reorientation and/or repositioning of users. To exploit SSID for user reorientation and repositioning, detection thresholds for scene rotations in the transverse plane and scene translations along the line of gaze in HMD setups remain to be tested.

2.2 Eye Movement Classification

Over the last decade, video-based eye trackers have established themselves as very reliable and easy to use. They provide clear prospects for miniaturization that will allow eye tracking within VR displays in the near future. However, fast video-based eye trackers, like the EyeLink from SR Research, are too bulky to be used with an HMD. Smaller devices, like the Arrington Research system are not fast enough to provide precise time-locking to saccade onsets. Electrooculography (EOG) amplifiers are small devices with high temporal-resolution. They measure the electric field created by the corneo-retinal resting potential with two skin electrodes placed on the head near the eyes. As the noise level of the EOG signal differs for each participant and may also differ over time, it is challenging to develop and setup a general eye movement classification algorithm.

Current eye movement classification approaches are mostly dispersion-based, velocity-based, acceleration-based or any combination of those [11, 15]. Dispersion-based algorithms detect fixations if the eye position stays within a spatial region of given visual angle for a certain time window [25]. Therefore, dispersion-based algorithms are sensitive to noise and drift in the eye position signal and lead to a considerable time lag, which makes it inapplicable for SSID. Velocity-based and acceleration-based algorithms classify data samples to belong to a saccade, when the eye velocity or acceleration exceeds a threshold. While simple algorithms using an empirically estimated constant threshold lead to a decrease in classification performance over time due to varying noise levels in EOG data, algorithms based on dynamic thresholds retain classification performance by adapting to the changes in the noise level. Duchowski [11] proposed an algorithm that dynamically estimates the acceleration threshold from the acceleration root mean square (RMS) during low velocity periods. The algorithm specifically amplifies regions of the eye velocity signal that are similar to an idealized saccade profile using a pattern-matching finite impulse response (FIR) filter. However, the FIR filter induces a considerable time lag of half the length of the idealized saccade profile, which makes it unsuitable for SSID. Nyström and Holmqvist [21] proposed an adaptive algorithm for fixation, saccade, and glissade detection that identifies saccades based on an iteratively updated peak velocity threshold. The peak velocity threshold is iteratively updated based on the mean and standard deviation of all samples below the current threshold until the change of the threshold between two consecutive updates is considerably small. Nevertheless, the focus on a peak velocity threshold makes it probably difficult to achieve saccade detection delays that are suitable for SSID, and the iterative threshold updates are computationally intensive.

Behrens et al. [2] suggested an algorithm that dynamically determines the acceleration threshold based on the standard deviation of the last 200ms. Thus, this algorithm is similar to the algorithm by Nyström and Holmqvist in terms of adapting the threshold based on the standard deviation. But, it is less computationally intensive, as there are efficient algorithms for determining a running standard deviation. Niemenlehto [20] presented a saccade detection algorithm that accomplishes a constant false alarm rate by adjusting a velocity threshold. For SSID, low and constant false alarm rates are important as every false alarm may lead to scene displacements that can be noticed by users.

3 Saccade Detection using Electrooculography

We modified the eye movement classification approaches from Behrens et al. and Niemenlehto (described in Section 2.2) to suit our needs for fast and reliable saccade detection. Afterwards, we assessed the modified saccade detection algorithms against a state-of-the-art video-based eye tracking system as ground truth. Based on the results of the assessment, we selected one algorithm for our study to investigate participants' sensitivity to scene translations and rotations during saccades. To ensure proper data acquisition during the experiment, we decided to use an additional calibration procedure to determine the best threshold parameters for each participant.

3.1 Saccade Detection Algorithms

3.1.1 Dynamic Acceleration Threshold Algorithm

Behrens et al. [2] proposed an algorithm for eye movement classification using a dynamic acceleration threshold (DAT). For data denoising, the eye position signal is low-pass filtered using a normalized windowed-sinc FIR filter to which a Hamming window is applied. The FIR filter has an odd filter length of $k+1, k \in \mathbb{N}$ samples and a cut-off frequency of $f_c \in \mathbb{R}$ Hz. Based on the denoised eye position signal, the eye acceleration signal is calculated using the differentiating FIR filter $\{1,-2,1\}$. Eye acceleration signal samples are classified as belonging to a saccade, whenever the eye acceleration signal sample exceeds the dynamic threshold $N\sigma \in \mathbb{R}$ with standard deviation $\sigma \in \mathbb{R}$ of the previous $\lambda \in \mathbb{R}$ seconds of the eye acceleration signal and a threshold parameter N that scales the standard deviation (see Figure 1(c)). During saccades, the acceleration threshold is not modified for 200ms and, afterwards, the threshold is slowly increased in a linear fashion until it intersects with the value of $N\sigma$ from which point on the acceleration threshold is dynamically calculated again. In case of artifacts the acceleration threshold does not have to be held constant and instead the dynamic threshold $N\sigma$ can be used to prevent many false alarms. Since

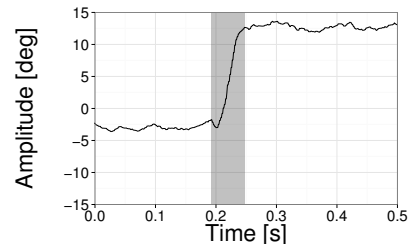

(a)

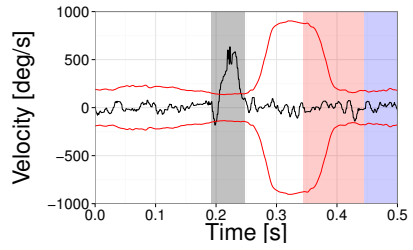

(b)

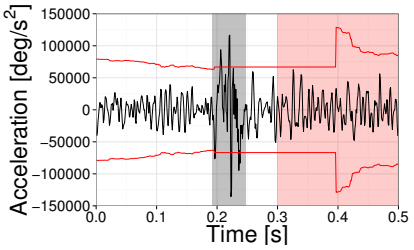

(c)

Fig. 1. Illustration of the modified saccade detection algorithms. (a) Electrooculography (EOG) signal for one exemplary saccade (light gray area). (b) The constant false alarm (CFAR) algorithm detects saccades when the eye velocity signal (black line) exceeds the dynamic threshold γ (red lines) for a certain period of time. For the next sample, the variance of the noise distribution is estimated from the mean velocity of the reference samples (light red area) in front of the guard samples (light blue area) to determine the dynamic threshold γ. (c) The dynamic acceleration threshold (DAT) algorithm detects saccades when the eye acceleration signal (black line) exceeds the dynamic threshold $N\sigma$ (red lines) for a certain period of time. For the next sample, the dynamic threshold is calculated from the standard deviation σ of the previous 200ms (light red area).

Behrens et al. do not mention the exact method to linearly increase the modified dynamic threshold $N\sigma$ in their paper, we held the threshold constant until 200ms are elapsed after the detection of the saccade offset. This is similar to the suggested method for biphasic saccades. In order to detect the saccade offset, the algorithm looks for the end of monotonicity in the eye position signal and in case of biphasic saccades the eye acceleration signal must be below the dynamic threshold $N\sigma$ in addition to the end of monotonicity. Behrens et al. use in their implementation the parameters $N = 3.4, \lambda = 0.2, k = 2\left\lfloor 0.7\frac{f_s}{f_c}\right\rfloor$ with sampling frequency $f_s \in \mathbb{R}$ Hz.

3.1.2 Constant False Alarm Rate Algorithm

Niemenlehto [20] suggested an eye movement classification algorithm that is based on the constant false alarm rate (CFAR) technique. The EOG signal may be preprocessed using low-pass or band-pass filters to reduce artifacts from facial musculature activity, high-frequency noise and power-line noise. The preprocessing may be unnecessary as, for instance, our EOG amplifiers already apply such denoising filters. The algorithm differentiates the EOG signal to derive the eye velocity signal using the two-point central difference FIR filter $v_i = \frac{x_i - x_{i-2p}}{2pT}$, where v_i is the i-th eye velocity sample, $T \in \mathbb{R}$ is the sampling interval in seconds and $p \in \mathbb{N}$ is the step size parameter. In the following we focus on the cell averaging method described by Niemenlehto, since it does not require the computationally expensive sorting of eye velocity samples as the order statistic method. Based on the assumption that the noise is normally distributed with zero mean (mean is removed by differentiation) and unknown variance σ^2, eye velocity samples that have a probability below $P_n \in \mathbb{R}$ of being noise are classified as saccades (see Figure 1(b)). Therefore, the eye velocity samples are tested against the dynamic threshold $\gamma = \sigma\sqrt{2/\pi}\sqrt{\pi}\,\mathrm{erf}^{-1}(1-P_n)$, where $\mathrm{erf}^{-1}(\cdot)$ is the inverse Gaussian error function. The variance (more precisely the standard deviation) is dynamically estimated for the i-th test sample as follows: $\sigma\sqrt{2/\pi} \approx r_i = \frac{1}{2q}\left(\sum_{k=-g-q}^{-g-1}|v_{i+k}| + \sum_{l=g+1}^{g+q}|v_{i+l}|\right)$ from $q \in \mathbb{N}$ reference samples with a margin of $g \in \mathbb{N}$ guard samples on each side of the tested eye velocity sample. Guard samples are used to avoid leakage of the higher variance during the beginning of saccades into the reference samples. There is a trade-off between low false alarm rate and high detection sensitivity, which is controlled by setting P_n. In order to provide a low value of P_n for high detection sensitivity while maintaining a low false alarm rate, the algorithm uses a rejection threshold γ_{rej} that rejects all saccades with less than γ_{rej} samples exceeding the dynamic threshold γ. The overall false alarm rate is $P = P_n^{\gamma_{\mathrm{rej}}}$ and different combinations of P_n and γ_{rej} yield the same overall false alarm rate. However, the greater the rejection threshold γ_{rej} the longer the duration until a saccade is detected, which must be considered for using the algorithm to exploit SSID. In order to detect the saccade offset, the algorithm looks for the eye velocity sample that is below the refraction threshold $\gamma_{\mathrm{ref}} = \sigma\sqrt{2/\pi}\sqrt{\pi}\,\mathrm{erf}^{-1}(1-0.5)$, which is equal to γ with $P_n = 0.5$. Niemenlehto used the parameters $p = 3, q = 100, g = 55, P_n = 0.1$ at 1000Hz sampling frequency for the evaluation of the algorithm.

3.1.3 Modifications for Online Saccade Detection

We omitted the calculation of saccade parameters such as amplitude and duration as we were mainly interested in applying scene changes as soon as saccades were detected. For the DAT algorithm, we transferred the rejection threshold from the CFAR algorithm to reject saccades when the acceleration signal did not exceed the threshold for γ_{rej} seconds to make the algorithm more robust against false alarms. Since our EOG amplifier introduced small signal changes in the opposite direction of the saccade at the saccade onset (see Figure 1(a)), we changed the monotonicity criteria to consider the real saccade direction and therefore ignore the artifact. For the CFAR algorithm, we considered only the guard and reference samples before the eye velocity test sample to avoid a considerable time lag of saccade detection that would render exploiting SSID impossible.

3.2 Assessment of Saccade Detection

We recorded the eye movements of three participants (2 male, 1 female, age: 28–30, $M = 28.7, SD = 1.2$) simultaneously with an AC EOG amplifier from biovision and an EyeLink 1000 from SR Research, which served as ground truth for the saccade detection. Participants sat in front of an Eizo FlexScan F930 22″ monitor with 1280×1024 pixels resolution and 100Hz refresh rate. Their head was fixed in a chin rest and the distance to the monitor was 57cm so that the screen corresponded to a visual field of $40^\circ \times 30^\circ$. For stimulus presentation, we used Psychtoolbox (Version 3) with Matlab from Mathworks (Version 2009*b*).

Participants had to perform 40 horizontal saccade trials for each amplitude ($3^\circ, 6^\circ, 9^\circ, 12^\circ, 24^\circ$) and 40 horizontal smooth pursuit trials for each speed ($10^\circ s^{-1}, 15^\circ s^{-1}, 20^\circ s^{-1}, 25^\circ s^{-1}, 30^\circ s^{-1}$) by looking at a red dot with a diameter of 0.25° visual angle. The direction of all saccades and smooth pursuits were counterbalanced to the left and right side for a total of 400 trials. The trials were all interleaved and presented in pseudo-random order. Participants performed saccades

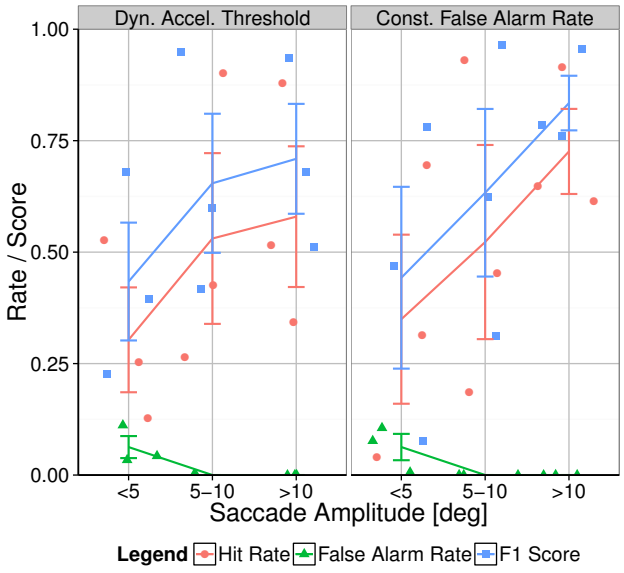

Fig. 2. Results of the dynamic acceleration threshold (DAT) and constant false alarm rate (CFAR) saccade detection algorithms assessment. Hit rates (red), false alarm rates (green), and F1 scores (blue) are shown for a conservative set of parameters (DAT: $N = 4$, CFAR: $P_n = 10^{-7}$, both: $\gamma_{\text{rej}} = 4$ms, denoising filter size 6ms). The error bars show ± 1 standard error of the mean. Horizontally jittered symbols represent the data of each individual participant. For the used set of parameters, both algorithms provide few false alarms even for small saccades while maintaining an acceptable hit rate. With increasing saccade amplitudes, false alarm rate is falling while the hit rate is rising.

700ms and smooth pursuit eye movements 1000ms after the start of the trial. After all trials, the screen went black for 700ms. We instructed participants to focus on the task and avoid blinks or unwanted eye movements except for the black screen intervals.

We assessed the hit rate (H), false alarm rate (F), and F1 score ($F1 = 2\frac{(1-F)\times H}{(1-F)+H}$) performance of the modified saccade detection algorithms for different sets of parameters. We set the size of the data denoising filter to 6ms, which we chose based on the suggestions of Bahil and McDonald [1] for two-point central difference filtering of EOG data and to keep the time delay caused by data filtering small. In addition, we required that all samples within $\gamma_{\text{rej}} = 4$ms have to exceed the threshold before a saccade is detected. We found that setting $N = 4$ for the DAT algorithm and $P_n = 10^{-7}$ for the CFAR algorithm provided good results if the false alarm rate must be low even for small saccades. Figure 2 shows the assessment results for small (< 5 degrees), medium (5–10 degrees) and large saccades (> 10 degrees) for this set of parameters. There were no false alarms for medium and large saccades and even for small saccades the algorithms showed a false alarm rate of approximately 6%. The hit rate increased with increasing saccade amplitude from approximately 30% (DAT) / 35% (CFAR) for small saccades to 65% (DAT) / 73% (CFAR) for large saccades. Based on the results, we used the CFAR algorithm due to its superior performance for our purposes although the DAT algorithm seemed to be slightly faster (as seen in informal data analysis).

We also found that the EOG noise-level differed substantially between participants and over time. Therefore, we decided to integrate a calibration procedure to determine the best threshold for each participant and each session in the study to investigate the sensitivity to scene rotations and translations during saccadic eye movements.

3.3 Calibration of Saccade Detection Threshold

During the calibration procedure, participants performed 10 saccades with an amplitude of 15° visual angle. We randomized the saccade direction, and jittered the saccade triggering time to be 1 ± 0.3 seconds after the trial start. Each trial had a duration of 2.5 seconds. The used saccade amplitude, saccade triggering timing and trial duration for the calibration procedure were equal to those of the sensitivity study.

We then determined the optimal threshold parameter P_n for the CFAR algorithm using a binary search. For each trial, we extracted the eye position signal 50ms to 500ms after the saccade triggering and determined the corresponding eye velocity signal using the FIR filter $\{-1, 1\}$. The saccade onset was determined for each trial by searching backwards in the eye velocity signal from the peak velocity towards the first sample below 5% of the peak velocity. We added a margin of 10ms to the saccade onset to avoid considering high eye velocity samples when the saccade onset was not detected properly. To determine the optimal threshold parameter P_n for the CFAR algorithm in terms of being the lowest possible parameter that causes no false alarm for the calibration saccades, we performed a binary search within the start interval $[0, 1]$ and chose the next interval depending on whether the CFAR algorithm produced a false alarm or not. Finally, we multiplied the parameter by 10^{-3} to make it more robust against false alarms, which is necessary as we only considered 10 saccades for the calibration procedure. In case of threshold parameters that would lead to an unacceptably high false alarm rate $P_n > 10^{-4}$ or to an unacceptably low detection sensitivity $P_n < 10^{-8}$, we discarded the threshold parameter and repeated the calibration procedure.

(a) (b)

Fig. 3. Illustration of the participant's instrumentation with virtual reality devices and the electrooculography (EOG) device. (a) Participants wore a head-mounted display to which an active infrared marker and orientation tracker was attached (Note: The black cloth to block vision of the real surrounding was removed for the illustration). Additionally, participants held a Nintendo Wii remote in their hand. (b) We placed silver chloride skin electrodes near the outer canthus of each eye and behind the participant's right ear.

4 Sensitivity to Scene Rotations and Translations

4.1 Participants

Ten participants (5 males, 5 females, age: 21–41, $M = 28.8, SD = 6.3$) took part in the sensitivity study. All participants were naïve to the experimental manipulation and had normal or corrected to normal vision (4 wore glasses, 2 wore contact lenses). None of the participants reported vestibular or stereopsis disorders. Six participants had much experience with HMDs and four participants had no to moderate HMD experience. Two participants stated much 3D game experience, two participants moderate and six participants no 3D game experience. Most participants were students or research associates with backgrounds in Psychology, Neuroscience, Computer Science and Fine Arts. Participants received neither monetary reward nor class credit, participated voluntarily and provided written consent.

(a) (b) (c) (d)

Fig. 4. Illustration of the participant's task for the sensitivity to scene rotations and translations study (Note: The red fixation cross is enlarged). (a) At the beginning of each trial participants looked straight at the red fixation cross and saw a view of the virtual replica of the laboratory room. (b) After 1 ± 0.3 seconds, the fixation cross changed its position and participants made a 15° saccade to the new position of the fixation cross. (c,d) The scene then rotated (c) or translated (d) and the fixation cross disappeared. The scene changed immediately when the saccade was detected in the scene change during saccades condition, while the scene changed after 0.3 ± 0.05 seconds in the scene change during fixations condition.

4.2 Instrumentation

An active infrared marker was attached to the head-mounted display (see Figure 3(a)). The Precision Position Tracking (PPT) X4 system from WorldViz ($<$ 1mm precision, $<$ 1cm accuracy, $<$ 20ms latency, 60Hz update rate) tracked the marker to determine the participant's position in world coordinate space. A wireless InertiaCube 3 orientation tracker from InterSense ($\leq 1^\circ$ accuracy, 4ms latency, 180Hz update rate) determined the participant's orientation.

We used an EOG amplifier from biovision to track the electric potential difference arising from horizontal eye movements. We attached one silver chloride electrode to the skin of participants at the outer canthus of each eye and the reference electrode on the skin behind the participant's right ear (see Figure 3(b)). The EOG amplifier was connected to the USB-1408 analog-digital converter board from Measurement Computing (14bit resolution, up to $48,000$ samples per second).

For EOG signal processing and rendering, we used a computer with 3.4GHz Intel Core i7 processor (16GB main memory) and Nvidia GeForce GTX 680 graphics card in surround screen mode for three displays with 3840×1024 pixels resolution. The virtual scene was rendered using OpenGL 4.3 and our own software. We displayed the virtual scene on the Sensics zSight head-mounted display (60° diagonal field of view, 2560×1024 pixels resolution, 60Hz update rate). On a LCD display we switched the background color to white when the virtual scene was changed due to a detected saccade. We monitored the exact timing of the scene change using a photosensitive diode, which we fixed on the LCD display and connected to the analog-digital converter board. Additionally, participants held a Nintendo Wii remote in their hand to make inputs for the experiment.

4.3 Procedure

After welcoming the participants and introducing the experimental procedure we measured the eye level of the participants and placed the EOG electrodes as described in Section 4.2. Then, participants put on and adjusted the HMD in order to see a sharp image. The laboratory room was darkened during the experiment and we wrapped a black cloth around the HMD to completely block any visual influence from the real environment. Participants received on-screen instructions about the task.

The study was divided into two blocks to investigate: (1) sensitivity to scene rotations, and (2) sensitivity to scene translations. We counter-balanced the order of the blocks and divided each block into three equal sessions, each consisting of a system calibration and a test phase. Participants were allowed to have breaks between the sessions and to perform the sessions on different days — mostly on two consecutive days separated by block.

In the calibration phase, participants pressed the action button on a Wii remote and then the yaw orientation and the head position was calibrated. Participants saw a photo-realistic virtual replica of the laboratory room on which we overlaid a red fixation cross with a size of 1° visual angle (see Figure 4(a)). Then, participants performed the threshold parameter calibration procedure for the CFAR algorithm as described in Section 3.3.

The test phase consisted of two conditions: scene changes (1) during saccades and (2) during fixations. Participants performed 84 trials for each condition (2 repetitions $\times$ 2 saccade directions $\times$ 21 types of rotation or translation), which resulted in a total of 168 trials for each test phase, and 504 trials for each study block (rotation or translation). We tested clockwise and counterclockwise rotation angles ranging from 0° to 10° visual angle in 1° visual angle steps as well as forward and backward translations ranging from 0m to 1.5m in 0.15m steps. All trials were presented randomly and uniformly distributed as we used the method of constant stimuli in a two-alternative forced-choice task (2AFCT).

For each trial, participants were virtually standing in the center of the virtual replica of the laboratory room, which was presented on the HMD (see Figure 4(a)). We randomized the yaw angle of the initial gaze orientation so that they saw a different view of the room in each trial. The task of the participants was to look directly at the overlaid fixation cross and, thus, to perform a 15° saccade when the position of the cross changed after 1 ± 0.3s (see Figure 4(b)). In case of the scene change during fixations condition, the scene was rotated or translated after another 0.3 ± 0.05s to prevent it from happening during the saccade. In case of the scene change during saccades condition, the scene was rotated or translated immediately when the saccade was detected. To make the saccade detection more robust against false alarms, we only considered saccades in the time window 50ms to 300ms after the position change of the fixation cross. The fixation cross disappeared at the same time when the scene was rotated (see Figure 4(c)) or translated (see Figure 4(d)) to prevent additional feedback about the scene change. The changed scene remained visible until 2.5s had passed since the start of the trial. Afterwards, participants had to press a button on the Wii remote to indicate whether they rotated to the left or right side for scene rotations. For scene translations, they indicated whether they moved forward or backward. When no saccade was detected in a scene change during saccade trial, the current trial was repeated. Otherwise, the next trial started.

At the end, the experimenter took off all devices and informally interviewed as well as debriefed participants. The total time per participant including instructions, training, experiment, breaks, questionnaires and debriefing took between 90 and 120 minutes.

4.4 Recorded Measures

We recorded the tracked position and orientation data with a sampling rate of 60Hz. The EOG, photodiode and saccade detection algorithm data was sampled at 1000Hz. In addition, we stored the answers of participants concerning the rotation or translation direction, the number of trial repetitions, and the trial parameters. In order to measure the degree to which our approach causes simulator sickness symptoms such as dizziness and nausea, participants filled out Kennedy's

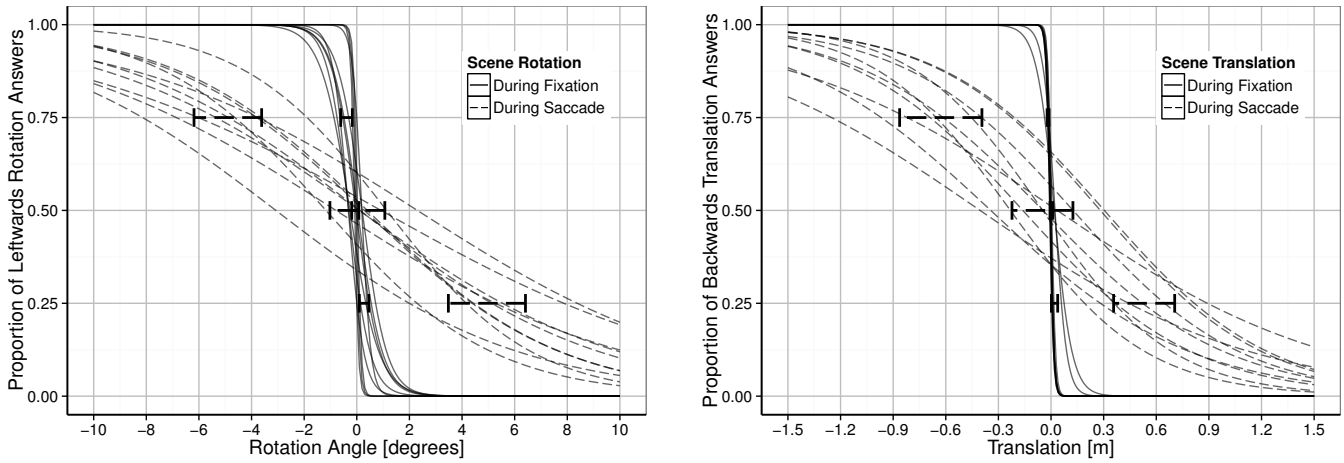

Fig. 5. Results of the sensitivity to scene rotations and translations study with ten participants for both conditions: scene changes during saccades (dashed lines) and during fixations (solid lines). (a) Individual proportion of leftwards rotation answers for each tested rotation angle and (b) of backwards translation answers for each tested translation. The lines show the non-linear least squares fits of the psychometric functions $f(x) = \frac{1}{1+e^{ax+b}}$, with $a,b \in \mathbb{R}$, to the individual data. The error bars show 95% confidence intervals for the points of subjective equality (PSEs) and the 75% detection thresholds (DTs).

Table 1. Mean points of subjective equality (PSEs) and 75% detection thresholds (DTs) for the sensitivity to scene rotations and translations study with ten participants for both conditions: scene changes during saccades and during fixations. Standard errors are given in parentheses.

	During Saccades			During Fixations		
	Lower DT	Upper DT	PSE	Lower DT	Upper DT	PSE
Rotations	$-4.90°$ $(0.57°)$	$4.95°$ $(0.65°)$	$0.02°$ $(0.46°)$	$-0.39°$ $(0.10°)$	$0.28°$ $(0.08°)$	$-0.06°$ $(0.06°)$
Translations	$-0.63m$ $(0.10m)$	$0.53m$ $(0.08m)$	$-0.05m$ $(0.08m)$	$-0.02m$ $(0.00m)$	$0.02m$ $(0.01m)$	$0.00m$ $(0.00m)$

simulator sickness questionnaire (SSQ) [17] before and after each experiment block. Participants, further, filled out the Slater-Usoh-Steed (SUS) presence questionnaire [35], and a questionnaire collecting demographic data and informal responses after the experiment.

4.5 Data Analysis

For statistical analysis, we used the R software (version 3.0.2) from R Foundation for Statistical Computing [23]. Significance was determined at the level of $p \leq 0.05$ for all comparisons. We tested the assumption that the data is normally distributed with the Shapiro-Wilk test. In case of non-normal distributions we verified the results using bootstrapping. The pre and post SSQ scores were tested for significant differences using the paired t-test. All questionnaires were additionally analyzed using the non-parametric Wilcoxon signed-rank test.

For the analysis of the sensitivity to scene rotations and translations during saccades and fixations, we determined the proportion of leftwards rotation and backwards translation for each condition and participant based on the 2AFCT answers of the participants. We fitted a psychometric function of the form $f(x) = \frac{1}{1+e^{ax+b}}$, with $a,b \in \mathbb{R}$ to the data for each participant and condition, using a non-linear least squares fit, in order to determine the point of subjective equality (PSE) and the 75% detection thresholds (DTs) [29]. For the PSEs and DTs, we analyzed if they were significantly different from zero for both conditions using one-sample t-tests and checked for significant differences between conditions using paired t-tests. Additionally, we examined significant differences between both conditions for the range between upper and lower detection thresholds using the paired t-test.

We investigated how often the experimental manipulation failed in the scene change during saccades condition. Therefore, we manually counted the number of false alarms in the EOG signal for each trial and determined the number of trials that were repeated due to missed saccades.

4.6 Results

4.6.1 Sensitivity to Scene Rotations

Figure 5(a) shows the individual proportion of leftwards rotation answers for each tested rotation angle and both conditions: scene change during saccades (dashed lines) and during fixations (solid lines). The lines indicate the fitted psychometric functions, which represent the sensitivity to scene rotations during saccades or fixations. The error bars show the 95% confidence intervals of the PSEs and DTs. Table 1 summarizes the mean PSEs and DTs derived from the psychometric functions fitted to the individual data of each participant. Standard errors are given in parentheses.

Participants were much more sensitive to scene rotations during fixations compared to scene rotations during saccades, $t(9) = -7.10, p < 0.0001, r = 0.92$ (upper DT), $t(9) = 7.70, p < 0.0001, r = 0.93$ (lower DT), $t(9) = -10.52, p < 0.0001, r = 0.96$ (range between DTs). Both DTs for scene rotations during saccades were significantly different from zero, $t(9) = 7.64, p < 0.0001, r = 0.93$ (upper DT), $t(9) = -8.63, p < 0.0001, r = 0.94$ (lower DT). Neither the PSE for scene rotations during fixations nor the PSE for rotations during saccades differed significantly from zero, $t(9) = -0.96, p = 0.36, r = 0.31$ (fixations), $t(9) = 0.05, p = 0.96, r = 0.02$ (saccades). Furthermore, the PSEs between the conditions were not significantly different, $t(9) = -0.18, p = 0.86, r = 0.06$. Over all participants, we quantified false alarms to be in the range from $2(0.8\%)$ to $29(11.5\%)$ $(M = 12.0(4.8\%), SE = 2.60(1.0\%), Mdn = 11(4.4\%))$. The number of repeated trials due to missed saccades ranged from 1 to 49 per participant $(M = 17.7, SE = 5.36, Mdn = 13.5)$.

4.6.2 Sensitivity to Scene Translations

Figure 5(b) shows the individual proportion of backwards translation answers for each tested translation and both conditions: scene change during saccades (dashed lines) and during fixations (solid lines). As for the sensitivity to scene rotations, the sensitivity to scene translations during saccades or fixations is determined using fitted psychometric functions that were plotted as lines. The error bars show the 95% confidence intervals of the PSEs and DTs. Table 1 summarizes the mean PSEs and DTs derived from the psychometric functions fitted to the individual data of each participant. Standard errors are given in parentheses.

Participants were also much more sensitive to scene translations during fixations compared to scene translations during saccades, $t(9) = -6.65, p < 0.0001, r = 0.91$ (upper DT), $t(9) = 5.91, p < 0.001, r = 0.89$ (lower DT), $t(9) = -11.07, p < 0.0001, r = 0.97$ (range between DTs). The upper and lower DT for scene translations during saccades differed significantly from zero, $t(9) = 6.90, p < 0.0001, r = 0.92$ (upper DT), $t(9) = -6.06, p < 0.001, r = 0.90$ (lower DT). The PSE for both scene translations during fixations and saccades were not significantly different from zero, $t(9) = 0.48, p = 0.64, r = 0.16$ (fixations), $t(9) = -0.6364, p = 0.54, r = 0.21$ (saccades). Additionally, the PSEs differed not significantly between the conditions, $t(9) = 0.67, p = 0.52, r = 0.22$. We quantified false alarms over all participants to be in the range from 3(1.2%) to 28(11.1%) ($M = 12.9(5.1\%), SE = 2.46(1.0\%), Mdn = 13(5.2\%)$). The number of repeated trials due to missed saccades ranged from 1 to 64 per participant ($M = 22.5, SE = 7.77, Mdn = 7.5$).

4.6.3 Questionnaires

The simulator sickness caused by the experiment was comparable for both scene rotations and translations. In the scene rotation block, there was a significant increase of the mean SSQ score from $M = 6.36$ ($SE = 2.9$) before to $M = 11.59$ ($SE = 3.27$) after the experiment, $t(9) = -2.58, p < 0.05, r = 0.65$. And, in the scene translation block, there was a non-significant trend for an increase of the mean SSQ score from $M = 9.72$ ($SE = 4.25$) before to $M = 15.33$ ($SE = 4.48$) after the experiment, $t(9) = -2.13, p = 0.06, r = 0.58$. We found that the average participants sense of presence score was $M = 4.8$ ($SE = 0.36$).

5 Discussion and Conclusions

The results of our sensitivity study show that applying trans-saccadic scene rotations and translations during SSID is a viable way to subliminally reorient and/or reposition the participant's viewpoint. Participants were considerably less sensitive to scene rotations and translations during saccades compared to scene changes during fixations. When standing still, participants approximately did not notice reorientations of $\pm 5^\circ$ in the transverse plane and repositioning of ± 0.5m along the line of gaze during saccades with an amplitude of 15°.

Several factors influence the sensitivity to scene changes during saccades, which need to be considered for a practical application. Participants are more sensitive to scene rotations orthogonal to the saccade than in the same direction as the saccade [19]. However, for trans-saccadic scene translations along the line of gaze with radial optic flow expansion patterns that provides deviations from the saccade in all possible directions, we still found a large range of possible manipulation that participants did not notice. The range of SSID scales with saccade amplitude [18]. As we used rather large saccades of 15° amplitude to ensure proper data acquisition in our study, we expect that the range must be reduced when saccades with smaller amplitudes should be considered for trans-saccadic scene changes. The saccade amplitude correlates with the saccade duration, which is also important for the sensitivity of scene changes, as participants are more sensitive to scene changes that are close to the saccade offset or shortly thereafter [10]. Assuming the linear relation found by Collewijn et al. [7] $d = 2.7a + 23$ with saccade durations $d \in \mathbb{R}$ in ms and saccade amplitudes $a \in \mathbb{R}$ in degrees, for small saccades of 3° the scene change must be applied in less than 31ms after the saccade onset. Thus, for the measured worst-case latency[1] of 22ms using the Sensics zSight HMD, there are still 9ms left for analog-to-digital signal conversion and saccade detection in order to apply the scene changes before the saccade offset. The distribution of saccade amplitudes/durations is task-specific and has to be considered for practical applications.

The average SSQ score was increased after the experiment, although the absolute post-SSQ scores were relatively low [17] and the difference between pre- and post-SSQ score is comparable to findings of redirected walking experiments [29]. Furthermore, the repeated use of the SSQ might lead to increased post-SSQ scores due to demand characteristics [38]. We therefore conclude that our approach did not cause unexceptional simulator sickness.

In the sensitivity study, we used a recognition task, in which participants had to state the direction of the scene rotation and translation, instead of a detection task, in which participants had to state if the scene had changed or had not changed. Theoretically, participants could be able to detect the scene change without being able to state the direction. However, as many participants asked if it is correct that in a lot of the trials the scene did not changed during the experiment, we think that it is unlikely that the results using a detection task will differ much from the results presented in this work, but this remains to be tested in a future experiment.

We modified two promising eye movement classification algorithms for the challenging task of fast online saccade detection. Since every saccade false alarm may lead to participants' noticing the scene change, it is important to keep the false alarm rate as low as possible. In the best case, the false alarm rate using the EOG approach should be comparable to the false alarm rate of state-of-the-art video-based eye tracking devices, which is currently impossible due to the higher level of noise in the EOG data. By tuning and optimizing the parameters of the modified saccade detection algorithms, we achieved a false alarm rate of approximately 6% for small saccades (amplitude $< 5^\circ$) for both algorithms. We selected the constant-false alarm rate algorithm for our sensitivity study due to the slightly superior hit rate performance ranging from 35% for small saccades to 73% for large saccades (amplitude $> 10^\circ$). In addition, we think that a constant-false alarm rate is a desirable feature to control how often participants will notice the manipulation. For fast online saccade detection to exploit SSID, there is a clear trade-off between the delay from saccade onset to detection and the performance in terms of hit rate and false alarm rate. Therefore, the algorithm performance is considerably better using lower thresholds when there is no need for fast detection. The performance for our modified version of the algorithm was comparable to simulations conducted by Niemenlehto with a 15dB saccade-to-noise power ratio (SNPR), $\gamma_{\text{rej}} = 7$ms and considerable lower threshold $P_n = 10^{-1}$, which resulted in an overall hit rate of 57.2%, false alarm rate of 6.5%, F1 score of 0.71. Because of the significant noise level in the EOG, which varies over time and participants, we had to perform per subject calibration of the saccade detection threshold in order to ensure proper data acquisition for our sensitivity study. In addition to the need for extensive tuning and parameter optimization for each participant, the EOG approach is rather cumbersome. In future experiments we plan to use new miniature high-speed video-oculography devices that provide a lower noise level, so that our approach can be used more efficiently and less intrusively.

Based on the results of this work, our approach to exploit SSID shows many opportunities for future research and applications to improve existing redirected walking and change blindness techniques. Therefore, we will investigate if our approach can be used during natural, unconstrained saccadic eye movements as users are exploring VEs by real walking. We plan to apply imperceptible trans-saccadic scene translations and rotations in addition to existing redirected walking techniques, to reduce the required space for unnoticeable redirected walking. This requires that we investigate the influence of a long series of successive trans-saccadic scene translations and rotations on the participant's sensitivity to detect those. Another interesting re-

[1] We measured the time until a photodiode registered the luminance change caused by switching the background color of the displays from black to white.

search question would be how much the required space for unnoticeable redirected walking can be reduced before users are unable to walk properly. Furthermore, to mask scene changes in visual illusion techniques [6] saccadic suppression may be used instead of the distracting gray screen. For change blindness approaches [31], saccadic suppression may be used to mask scene changes such as the replacement of a door even when the door is in the user's visual field of view.

ACKNOWLEDGMENTS

Authors of this work were supported by the Deutsche Forschungsgemeinschaft (DFG 29160962).

REFERENCES

[1] A. T. Bahill and J. D. McDonald. Frequency limitations and optimal step size for the two-point central difference derivative algorithm with applications to human eye movement data. *IEEE Trans. Bio-Med. Engin.*, 30(3):191–194, 1983.

[2] F. Behrens, M. MacKeben, and W. Schröder-Preikschat. An improved algorithm for automatic detection of saccades in eye movement data and for calculating saccade parameters. *Behav. Res. Methods*, 42(3):701–708, 2010.

[3] L. Bouguila, M. Sato, S. Hasegawa, H. Naoki, N. Matsumoto, A. Toyama, J. Ezzine, and D. Maghrebi. A new step-in-place locomotion interface for virtual environment with large display system. In *Proc. SIGGRAPH*, page 63. ACM, 2002.

[4] B. Bridgeman, D. Hendry, and L. Stark. Failure to detect displacement of the visual world during saccadic eye movements. *Vis. Res.*, 15(6):719–722, 1975.

[5] G. Bruder, F. Steinicke, B. Bolte, P. Wieland, H. Frenz, and M. Lappe. Exploiting perceptual limitations and illusions to support walking through virtual environments in confined physical spaces. *Displays*, 34(2):132–141, 2013.

[6] G. Bruder, F. Steinicke, P. Wieland, and M. Lappe. Tuning self-motion perception in virtual reality with visual illusions. *IEEE Trans. Visual. Comput. Graph. (TVCG)*, 18(7):1068–1078, 2012.

[7] H. Collewijn, C. J. Erkelens, and R. M. Steinman. Binocular coordination of human horizontal saccadic eye movements. *J. Physiol.*, 404:157–182, 1988.

[8] H. Deubel, B. Bridgeman, and W. X. Schneider. Immediate post-saccadic information mediates space constancy. *Vis. Res.*, 38(20):3147–3159, 1998.

[9] H. Deubel, W. X. Schneider, and B. Bridgeman. Postsaccadic target blanking prevents saccadic suppression of image displacement. *Vision Res.*, 36(7):985–996, 1996.

[10] M. R. Diamond, J. Ross, and M. C. Morrone. Extraretinal control of saccadic suppression. *J. Neurosci.*, 20:3449–3455, 2000.

[11] A. T. Duchowski. *Eye Tracking Methodology - Theory and Practice*. Springer, second edition, 2007.

[12] T. Field and P. Vamplew. Generalised algorithms for redirected walking in virtual environments. In *Proc. Artif. Intell. Sci. Techn.*, AISAT '04, pages 58–63, 2004.

[13] J. Grimes. On the failure to detect changes in scenes across saccades. In K. Akins, editor, *Vancouver studies in cognitive science*, volume 5, chapter Perception 4, pages 89–110. New York: Oxford Universitiy Press, 1996.

[14] R. Herpers, J. Schumacher, and R. S. Allison. Hiding graphic updates during long saccadic suppression periods. In *Dyn. Percept.*, pages 77–82, 2004.

[15] K. Holmqvist, M. Nyström, R. Andersson, R. Dewhurst, H. Jarodzka, and J. van de Weijer. *Eye Tracking: A Comprehensive Guide to Methods and Measures*. Oxford, first edition, 2011.

[16] H. Iwata, H. Yano, and H. Tomioka. Powered shoes. In *Proc. SIGGRAPH*, SIGGRAPH '06, New York, NY, 2006. ACM Press.

[17] R. Kennedy, N. Lane, K. Berbaum, and M. Lilienthal. Simulator sickness questionnaire: An enhanced method for quantifying simulator sickness. *Int. J. Aviat. Psychol.*, 3(3):203–220, 1993.

[18] W. Li and L. Matin. The influence of saccade length on the saccadic suppression of displacement detection. *Percep. Psychophys.*, 48(5):453–458, 1990.

[19] M. Niemeier, J. D. Crawford, and D. B. Tweed. Optimal transsaccadic integration explains distorted spatial perception. *Nature*, 422(6927):76–80, 2003.

[20] P.-H. Niemenlehto. Constant false alarm rate detection of saccadic eye movements in electro-oculography. *Comput. Methods. Programs Biomed.*, 96(2):158–171, 2009.

[21] M. Nyström and K. Holmqvist. An adaptive algorithm for fixation, saccade, and glissade detection in eyetracking data. *Behav. Res. Methods*, 42(1):188–204, 2010.

[22] T. C. Peck, H. Fuchs, and M. C. Whitton. Evaluation of reorientation techniques and distractors for walking in large virtual environments. *IEEE Trans. Visual. Comput. Graph. (TVCG)*, 15(3):383–394, 2009.

[23] R Core Team. *R: A Language and Environment for Statistical Computing*. R Foundation for Statistical Computing, Vienna, Austria, 2013.

[24] S. Razzaque. *Redirected Walking*. PhD thesis, University of North Carolina, Chapel Hill, 2005.

[25] D. D. Salvucci and J. H. Goldberg. Identifying fixations and saccades in eye-tracking protocols. In *Proc. Eye Track. Res. Appl.*, ETRA '00, pages 71–78, New York, NY, USA, 2000. ACM.

[26] J. Schumacher, R. S. Allison, and R. Herpers. Using saccadic suppresion to hide graphic updates. In *Proc. Eurograph.*, EGVE '04, pages 17–24. ACM Press, 2004.

[27] M. Schwaiger, T. Thümmel, and H. Ulbrich. A 2d-motion platform: The cybercarpet. In *Proc. Joint EuroHaptics Conf. and Symp. Hapt. Interf. Virt. Env. and Teleop. Syst.*, 2007.

[28] J. L. Souman, P. R. Giordano, M. Schwaiger, I. Frissen, T. Thümmel, H. Ulbrich, A. D. Luca, H. H. Bülthoff, and M. O. Ernst. Cyberwalk: Enabling unconstrained omnidirectional walking through virtual environments. *ACM Trans. Appl. Percept.*, 8(4):25:1–25:22, 2008.

[29] F. Steinicke, G. Bruder, J. Jerald, H. Frenz, and M. Lappe. Estimation of detection thresholds for redirected walking techniques. *IEEE Trans. Visual. Comput. Graph.*, 16(1):17–27, 2010.

[30] E. A. Suma, G. Bruder, F. Steinicke, D. M. Krum, and M. Bolas. A taxonomy for deploying redirection techniques in immersive virtual environments. In *Proc. Virt. Real.*, VR '12, pages 43–46, Washington, DC, 2012. IEEE Computer Society.

[31] E. A. Suma, S. Clark, D. Krum, S. Finkelstein, M. Bolas, and Z. Warte. Leveraging change blindness for redirection in virtual environments. In *Proc. Virt. Real.*, VR '11, pages 159–166, Washington, DC, USA, 2011. IEEE Computer Society.

[32] M. Suryajaya, T. Lambert, C. Fowler, P. Stothard, D. Laurence, and C. Daly. OmniWalker: omnidirectional stroller-based walking platform. In *Proc. Virt. Real. Int. Conf.*, VRIC 10, pages 181–182, 2010.

[33] J. Triesch, B. T. Sullivan, M. M. Hayhoe, and D. H. Ballard. Saccade contingent updating in virtual reality. In *Proc. Eye Track. Res. Appl.*, ETRA '02, pages 95–102. ACM Press, 2002.

[34] M. Usoh, K. Arthur, M. C. Whitton, R. Bastos, A. Steed, M. Slater, and F. P. Brooks, Jr. Walking > walking-in-place > flying, in virtual environments. In *Proc. SIGGRAPH*, SIGGRAPH '99, pages 359–364, New York, NY, 1999. ACM Press/Addison-Wesley Publishing Co.

[35] M. Usoh, E. Catena, S. Arman, and M. Slater. Using presence questionnaires in reality. *Presence-Teleop. Virt.*, 9(5):497–503, 1999.

[36] B. Williams, G. Narasimham, T. P. McNamara, T. H. Carr, J. J. Rieser, and B. Bodenheimer. Updating orientation in large virtual environments using scaled translational gain. In *Proc. Appl. Percept. Graph. Visual.*, volume 153 of *APGV '06*, pages 21–28. ACM Press, 2006.

[37] B. Williams, G. Narasimham, B. Rump, T. P. McNamara, T. H. Carr, J. J. Rieser, and B. Bodenheimer. Exploring large virtual environments with an hmd on foot. In *Proc. Appl. Percept. Graph. Visual.*, volume 153 of *APGV '06*, pages 148–148. ACM Press, 2006.

[38] S. D. Young, B. D. Adelstein, and S. R. Ellis. Demand characteristics in assessing motion sickness in a virtual environment: Or does taking a motion sickness questionnaire make you sick? *IEEE Trans. Visual. Comput. Graph. (TVCG)*, 13(3):422–428, 2007.